ARTICLE OPEN ACCESS

Corrosion Behavior of Commercial FeCrAl and TiAl Alloys in Molten Pb With 2E-7 wt% Oxygen at 600°C and 700°C

Renate Fetzer | Anisa Purwitasari | Annette Heinzel | Alfons Weisenburger | Georg Müller

Institute for Pulsed Power and Microwave Technology (IHM), Karlsruhe Institute of Technology (KIT), Karlsruhe, Germany

Correspondence: Renate Fetzer (renate.fetzer@kit.edu)

Received: 9 February 2026 | **Revised:** 26 May 2026 | **Accepted:** 22 June 2026

Funding: Bundesministerium für Wirtschaft und Klimaschutz, Grant/Award Number: 03EE5050C

Keywords: corrosion | dissolution | ferritic FeCrAl | liquid lead | oxidation | titanium aluminide

ABSTRACT

Liquid lead (Pb) is an attractive heat transfer fluid for advanced thermal energy storage (TES) systems. In the search for adequate structural materials that withstand the corrosive nature of liquid Pb at high temperature, Al-containing materials might offer excellent corrosion resistance due to their ability to form protective alumina scales. This study investigates the corrosion behavior of two commercial ferritic FeCrAl alloys, Kanthal APM and Kanthal APMT, and two titanium aluminides, TNM-B1 and GE 48-2-2, in liquid Pb under conditions relevant for TES systems. Exposure tests are performed in liquid Pb with 2E-7 wt.% dissolved oxygen at 600°C and 700°C for up to 5000 h. Examination of the specimens after exposure shows the formation of stable and protective oxide scales at 600°C on all materials, while exposure at 700°C leads to various failure mechanisms, ranging from internal oxidation for APM to severe Pb penetration for TNM-B1 and GE 48-2-2.

1 | Introduction

Heavy liquid metals such as liquid lead (Pb) are attractive heat transfer media for advanced thermal energy storage (TES) systems due to their excellent heat conductivity and wide temperature stability range [1–3]. In contrast to light metals such as Na, liquid Pb is chemically inert and offers high safety. The main drawback of heavy liquid metals is their high aggressiveness towards structural materials due to the high solubility of steel alloying elements (Fe, Cr, Ni) in the liquid metals at high temperature. Here, liquid Pb offers some advantages over liquid Sn, for instance, due to the lower solubility. Additionally, Pb does not form intermetallic phases with the alloying elements, which could further accelerate the corrosion process. A typical strategy to mitigate dissolution corrosion in liquid Pb is the active control of oxygen dissolved in the liquid metal to enable the formation of a continuous and protective oxide scale [4, 5]. Hereby, the properties of the formed oxide scale and its protectiveness and self-healing capabilities depend on the exposure temperature, the dissolved oxygen concentration, and on the composition and microstructure of the structural material. At rather low temperature, i.e., up to about 550°C, the growth rate of oxide scales is quite low even at high oxygen concentration. For Fe-based alloys (steels), this typically results in a duplex oxide scale with outward-growing magnetite and inward-growing Fe-Cr-spinel [5–8]. Although magnetite might become porous and spall off for prolonged exposure, the underlying spinel remains dense and protective. As temperature increases, the oxidation rate is enhanced and Fe-Cr-spinel-based oxide scales become less dense and lose their protective properties for temperatures around 600°C and above. This can result in inward growing oxidation, selective dissolution, and penetration of Pb [9–12]. Therefore, for high temperature applications, stronger oxide formers such as Al need to be added to the material in

sufficient amounts or in the form of an Al-containing coating. Selective oxidation of Al then enables the formation of a slowly-growing dense alumina scale that remains protective even for prolonged exposure at high temperature [13–20].

The present study focuses on commercially available Al-containing bulk materials. One example of commercial alumina-forming materials is the family of ferritic FeCrAl alloys. The alloys Kanthal AF, Kanthal APM, and Kanthal APMT have been specifically designed for high-temperature applications, offering excellent mechanical strength and oxidation resistance. All three alloys contain the same nominal amount of Cr (20.5–23.5 wt.%) and minor additions of C, Si, and Mn. The Al content varies slightly (AF: 5.3 wt.%, APM: 5.8 wt.%, APMT: 5.0 wt.%), while Mo (3.0 wt.%) is added to APMT only. In the past decades, the corrosion behavior of these alloys has been studied widely in lead-bismuth eutectic (LBE) to investigate their potential use in advanced GEN IV lead-cooled fast reactors [21–24]. At 500°C to 600°C, except for some local deviations (oxides other than alumina on APM at 500°C, local Pb penetration on AF at 550°C), a thin protective alumina scale had formed on AF and APM after 1000 h exposure to LBE with dissolved oxygen concentrations ranging from 1E-8 to 1E-6 wt.% [21, 22]. At 700°C and 750°C, APM and APMT (700°C) and AF and APM (750°C) also showed the growth of a thin protective alumina scale after 1000 h for oxygen contents of at least 1E-6 wt.%, while an oxygen content of 1E-8 wt.% was not sufficient to protect AF and APM from dissolution corrosion in LBE at 750°C [22, 24]. At 800°C, dissolution corrosion of APM and APMT was observed for both low oxygen concentration (2E-7 wt.%) and higher oxygen contents (1E-6 to 1E-4 wt.%), in the latter case in combination with the formation of thick oxides, spallation, and internal oxidation [23, 24].

Corrosion studies on APM and APMT in pure liquid Pb are available for high temperatures only, i.e., for 750°C to 900°C [14, 19]. At 800°C and with an oxygen content of 1E-5 wt.%, the growth of a thin alumina scale and locally some internal oxidation was found on APM, while APMT showed a continuous corrosion attack with internal oxidation and Pb penetration after 1760 h [14]. Both materials showed continuous corrosion at 900°C [14]. At 750°C, dissolved oxygen concentrations of both 4E-7 wt.% and 2E-6 wt.% were found to result in the formation of a thin alumina scale on APMT, with some local thicker oxide nodules and Pb penetration found after 2000 h of exposure to Pb with 2E-6 wt.% oxygen [19]. In the present study, the two ferritic FeCrAl alloys Kanthal APM and Kanthal APMT were selected, and their corrosion behavior in liquid Pb at 600°C and 700°C was investigated for up to 5000 h. For the corrosion tests, a concentration of 2E-7 wt.% dissolved oxygen was used, which corresponds to the value envisaged for TES applications.

The second group of commercial Al-containing bulk materials investigated in the present study are titanium aluminides. TiAl alloys are typically used in the aerospace industry due to their lightweight. The mechanical properties are largely determined by their microstructure, which strongly depends on both the composition and the manufacturing route [25]. In high-temperature gaseous atmospheres, γ-TiAl alloys typically form multi-layered oxide scales consisting of TiO_2 and Al_2O_3 [26]. Hereby, TiO_2 is less dense and thus less favorable, while Al_2O_3 has the potential to form a dense protective scale. To promote the formation of Al_2O_3 over that of TiO_2, small amounts of Nb, Cr, or Mo are typically added to the TiAl alloys. Although a wide knowledge exists on the high-temperature oxidation behavior of titanium aluminides in gas atmospheres, only one study is available on the corrosion behavior of this material family in heavy liquid metals [27]. $Ti_{48.5}Al_{46}Cr_3Nb_{0.5}Mo_2$ alloy with and without pre-oxidation was tested in LBE for 500 and 1000 h at 550°C in a closed quartz tube without gas control. The microstructure of the material consisted of a γ-TiAl matrix and CrMo-rich precipitations (σ phase) formed at high temperature. Samples without pre-oxidation showed severe corrosion attack. Hereby, the LBE penetrated preferentially via the CrMo-rich phase, which was identified as the weak point of the alloy regarding its corrosion resistance. For the present study, two commercial representatives of the family of γ-TiAl alloys were selected, TNM-B1 and GE 48-2-2. These materials contain either Cr (GE 48-2-2) or Mo (TNM-B1) but not both alloying elements at the same time. As the FeCrAl alloys, specimens from the γ-TiAl alloys were exposed to liquid Pb containing 2E-7 wt.% dissolved oxygen for up to 5000 h at 600°C and 700°C to study the corrosion behavior and material compatibility under conditions relevant for TES applications with liquid Pb as heat transfer fluid.

2 | Materials and Methods

The nominal composition of the dispersion-strengthened ferritic FeCrAl alloys Kanthal APM and Kanthal APMT is given in Table 1. The main differences in composition are the slightly higher Al content of APM and the addition of Mo to APMT. Regarding the microstructure, APMT contains an increased amount of finely dispersed stable inclusions (mainly oxides, but also carbides and nitrides), which improve the high-temperature strength and creep properties [28].

From the family of γ-TiAl alloys, the materials TNM-B1 and Ti-48Al-2Cr-2Nb (patented by General Electric; short name: GE 48-2-2) were selected, see Table 2 for nominal compositions. Generally, the main phase constituents of titanium aluminides are γ-TiAl, α_2-Ti_3Al, and β_0 (Cr-, Mo-rich phase promoted by the presence of Nb). Typical microstructures consist of α_2/γ lamellar colonies and pure-phase grains in various ratios. According to GfE Metalle und Materialien GmbH, the microstructure of TNM-B1 consists of α_2/γ lamellar colonies, globular

TABLE 1 | Nominal composition of FeCrAl alloys Kanthal APM and Kanthal APMT (in wt.%). Both FeCrAl alloys additionally contain reactive elements such as Y, Ti, Hf, and Zr.

	C	Si	Mn	Mo	Cr	Al	Fe
APM	≤ 0.08	≤ 0.7	≤ 0.4	—	20.5–23.5	5.8	Bal.
APMT	≤ 0.08	≤ 0.7	≤ 0.4	3.0	20.5–23.5	5.0	Bal.

TABLE 2 | Nominal composition of γ-TiAl alloys TNM-B1 and GE 48-2-2 (in at%). Both γ-TiAl alloys may contain impurities from H, N, O, C, Fe, Ni.

	Ti	Al	Cr	Nb	Mo	B
TNM-B1	Bal.	43.5	—	4	1	0.1
GE 48-2-2	Bal.	48	2	2	—	—

β/B2 grains, globular γ-TiAl grains, and globular α_2-Ti_3Al grains, while the microstructure of GE 48-2-2 consists of extended α_2/γ lamellar colonies and small amounts of γ-grains, α_2-grains, and β_0-grains.

Lead (Pb, purity 99.995%) was obtained from HMW Hauner GmbH Co. KG in the shape of bars. The Pb was melted and poured into alumina crucibles for the exposure tests. The materials to be tested were cut into rectangular specimens (FeCrAl alloys: 28 × 10 × 3 mm, γ-TiAl alloys: 20 × 10 × 1.5 mm). Prior to exposure, the specimen surfaces were ground with #1200 SiC paper and cleaned with ethanol. The static exposure tests in molten Pb with a controlled content of 2E-7 wt.% dissolved oxygen were performed in the COSTA facility [7] at two different temperatures, 600°C and 700°C, for up to 5000 h, see Table 3 for the specific exposure times. Each exposure duration was realized in an individual experiment to avoid oxygen ingress during sample extraction. To achieve and control the target amount of dissolved oxygen, a continuous flow of a gas mixture with specific H_2/H_2O ratio was used. The actual oxygen content was between 1E-7 and 2E-7 wt.% during the tests performed at 600°C and between 1E-7 and 5E-7 wt.% during the 700°C tests. Each specimen was exposed in an individual Pb-filled crucible. The ratio of the exposed specimen surface to the liquid Pb volume was below 270 cm^2/L for all samples.

After extracting from the COSTA facility, the samples were allowed to cool to ambient temperature in controlled atmosphere. Each specimen was subsequently cut into two parts. One part was allocated for cross-sectional analysis and embedded in resin without prior surface cleaning. Metallographic preparation was carried out by grinding with SiC paper up to 2400 grit, followed by polishing with a diamond suspension to a final particle size of 1 µm. The prepared cross-sections were examined using Scanning Electron Microscopy (SEM, Zeiss LEO 1530 VP) to investigate the corrosion behavior. Energy Dispersive X-ray Spectroscopy (EDS) was used to determine the elemental distribution and composition. The second part of the TNM-B1 samples was cleaned from adherent lead and analyzed by X-ray Diffraction (XRD, Seifert 3003 PTS) to identify the crystalline phases of the corrosion products.

3 | Results and Discussion

3.1 | FeCrAl Alloys

3.1.1 | APM

APM develops an ultra-thin, Al-rich oxide scale after 1000 and 2000 h of exposure to liquid lead with 2E-7 wt.% dissolved oxygen at 600°C (Figure 1a). The sample shows no evidence of

TABLE 3 | Materials and exposure times of corrosion tests in liquid Pb containing 2E-7 wt.% dissolved oxygen.

	600°C			700°C		
Material	**1000 h**	**2000 h**	**5000 h**	**1000 h**	**2000 h**	**5000 h**
APM	✓	✓	✓	✓	✓	✓
APMT	✓	✓		✓	✓	
TNM-B1		✓	✓		✓	✓
GE 48-2-2	✓	✓		✓	✓	

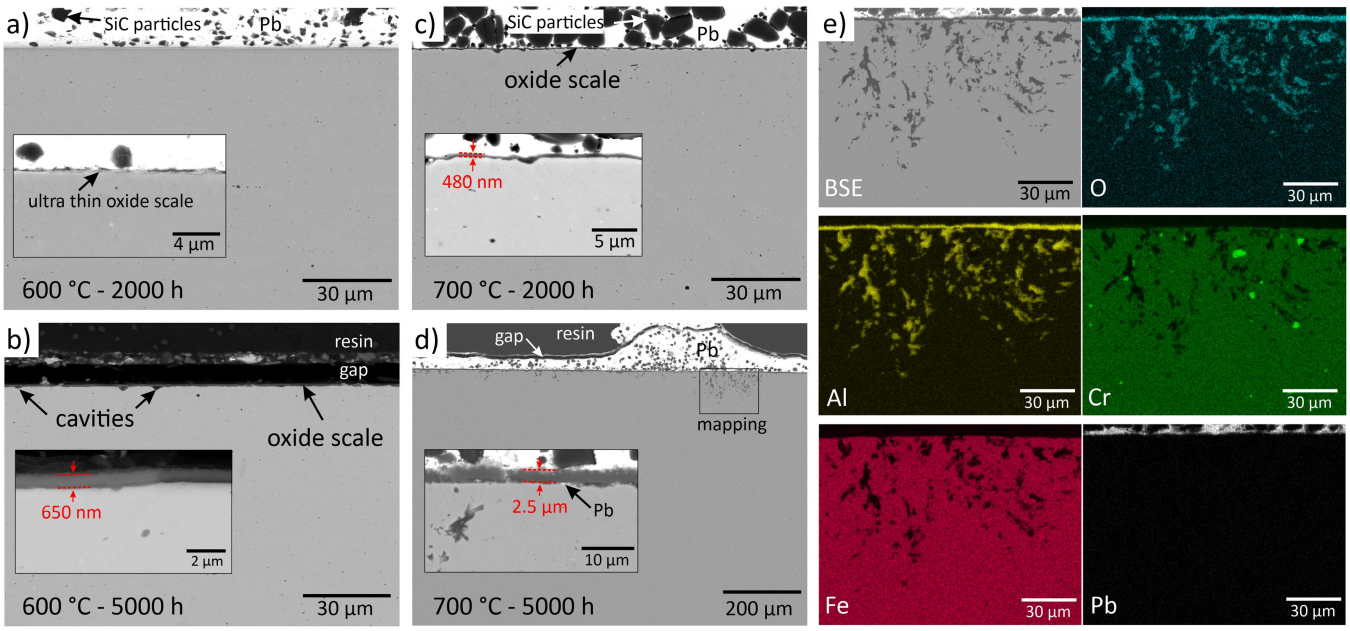

FIGURE 1 | APM after 2000 h (a, c) and 5000 h (b, d) exposure to liquid Pb at 600°C (a, b) and 700°C (c, d), respectively. (e) EDS elemental mapping of the selected area marked in (d). The SiC particles in these and all further images stem from the SiC paper used for grinding. [Color figure can be viewed at wileyonlinelibrary.com]

localized liquid lead penetration or inward-growing oxide, indicating that the aluminum-rich scale serves as an effective diffusion barrier. After prolonged exposure for 5000 h, excellent corrosion resistance is retained, with oxide growth reaching a scale thickness of 580–700 nm (Figure 1b). Some cavities are occasionally observed beneath the oxide scale, but they remain localized and do not compromise the continuity of the protective layer throughout the 5000-h exposure.

Exposure of APM to Pb at 700°C for 2000 h (Figure 1c) results in the formation of an Al-rich oxide layer approximately 420–500 nm thick, significantly thicker than that formed at 600°C, which shows accelerated oxidation kinetics at the higher temperature. Significant changes in corrosion behavior develop after 5000 h of exposure. As shown in Figure 1d, the oxide layer thickened considerably (values in the range 2.0–3.0 μm are found), and internal oxidation is observed. The EDS mapping in Figure 1e confirms formation of intergranular Al-oxide. These results show that the oxide scale is not protective any more after 5000 h, likely due to the excessive thickness compromising its stability and resulting in defects such as porosity, microcracks, and localized spallation, which facilitates inward oxygen diffusion and, potentially, lead penetration. Intergranular oxides extend to depths of approximately 100 μm. No evidence of lead penetration is detected.

3.1.2 | APMT

Figure 2a shows the cross-section of APMT after exposure to liquid Pb at 600°C for 2000 h. The alloy developed an extremely thin, continuous Al-rich oxide layer. No evidence of localized corrosion attack or internal oxidation is detected, indicating that the scale is protective—at least in the first 2000 h of exposure. At the higher temperature of 700°C, the oxide thickness increased substantially, reaching values up to 680 nm after 2000 h (Figure 2b). The oxide scale is protective for 2000 h also at higher temperature.

3.2 | Discussion of FeCrAl Alloys

Both commercial FeCrAl alloys APM and APMT form a thin and protective Al-rich oxide scale in molten Pb with 2E-7 wt.% dissolved oxygen for exposures up to 2000 h at 600°C and 700°C. These results are in agreement with the literature on the oxidation/corrosion behavior of these alloys in LBE in the same temperature range. After 1000 h of exposure to LBE at 600°C, a thin protective alumina scale was found on APM (1E-8 to 1E-6 wt.% dissolved oxygen) [22], and at 700°C, an Al-rich oxide was observed on both APM and APMT (1E-6 wt.% oxygen, 1000 h) [24]. Furthermore, the present results are in agreement with reported exposure tests of APMT in liquid Pb at a slightly higher temperature of 750°C, where an oxygen content of 4E-7 wt.% resulted in the formation of a protective alumina scale after 650 h [19]. At a higher oxygen content of 2E-6 wt.%, some thicker oxide nodules and Pb penetration were observed locally after 2000 h [19].

In the present study, the alloy APMT developed a slightly thicker scale within the timescale of 2000 h (up to 680 nm at 700°C) than the alloy APM (420–500 nm at 700°C), which shows a slightly accelerated oxidation kinetics on APMT. This might be related to the presence of Mo or the deviating microstructure. An accelerated oxidation kinetics might lead to an earlier failure of the scale as reported for corrosion tests in Pb with 1E-5 wt.% dissolved oxygen at 800°C. Here, a clear corrosion attack was observed for APMT after 1760 h, while APM showed better corrosion resistance with Al-oxide scale formation and merely local internal oxidation [14].

The present results obtained for APM for the exposures to liquid Pb exceeding 2000 h show a crucial difference between the two exposure temperatures tested in this study. At 600°C, the growth of the thin oxide scale continues and the scale remains protective for at least 5000 h. At 700°C, however, the corrosion behavior starts to deviate from the described behavior. Upon further growth to a thickness of around 2–3 μm after 5000 h, the oxide scale became unstable and internal oxidation occurred. The even faster scale growth on APMT in the first 2000 h suggests the same fate for prolonged exposure of APMT to Pb at 700°C. Also here, the oxide scale might lose its protective properties after 5000 h, leading to local spallation and internal oxidation.

Since previously reported studies did not exceed an exposure time of 2000 h, these new findings are of great relevance for the assessment of the long-term corrosion resistance of FeCrAl alloys to liquid Pb. Excellent corrosion protection is obtained at 600°C, while the corrosion resistance deteriorates after 5000 h at 700°C.

3.3 | TiAl Alloys

3.3.1 | TNM-B1

As shown in Figure 3, the γ-TiAl alloy TNM-B1 developed a continuous oxide layer after exposure to liquid lead at 600°C.

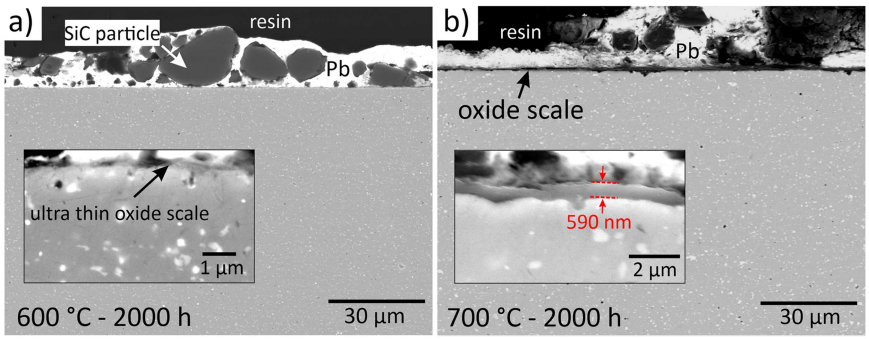

FIGURE 2 | APMT after 2000 h exposure to liquid Pb (a) at 600°C, (b) at 700°C. [Color figure can be viewed at wileyonlinelibrary.com]

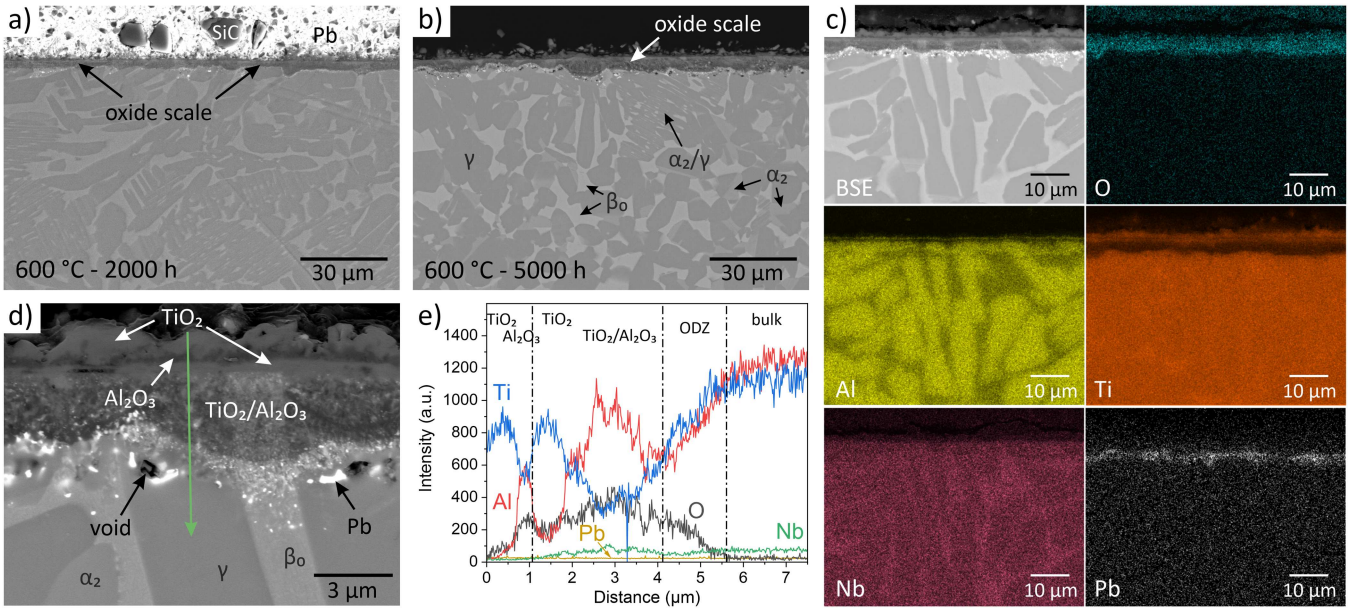

FIGURE 3 | TNM-B1 after exposure to liquid Pb at 600°C (a) for 2000 h, (b–d) for 5000 h. (a, b) BSE images, (c) EDS elemental mapping, (d) BSE image at higher magnification, (e) result of EDS elemental line scan along arrow in (d). [Color figure can be viewed at wileyonlinelibrary.com]

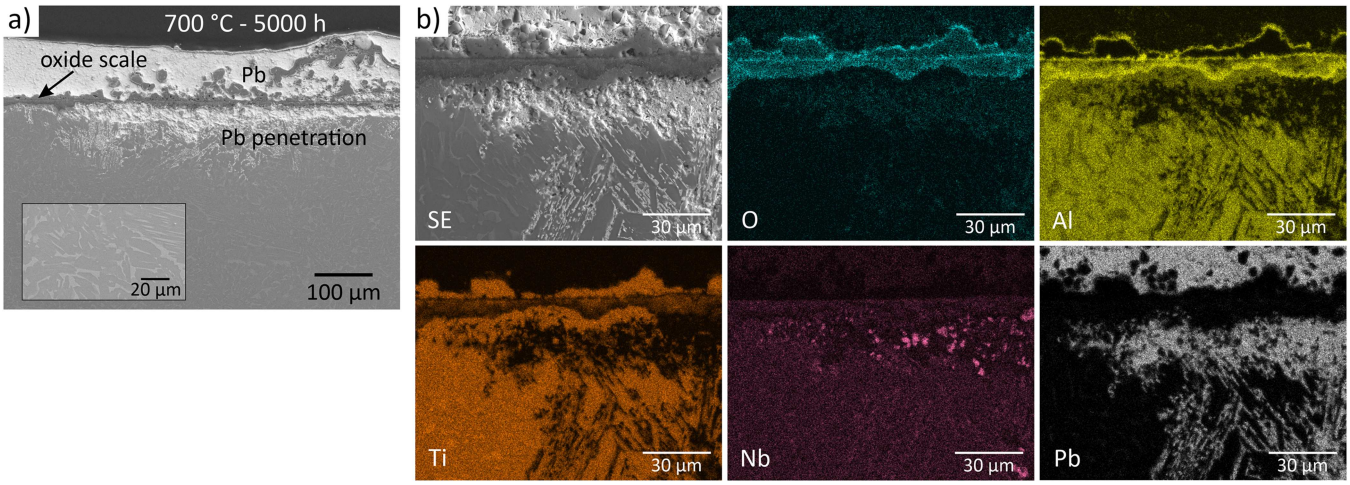

FIGURE 4 | TNM-B1 after 5000 h exposure to liquid Pb at 700°C: (a) SE image (inset: bulk microstructure), (b) EDS elemental mapping. [Color figure can be viewed at wileyonlinelibrary.com]

The scale has a total thickness of about 3–3.5 µm after 2000 h (Figure 3a) and grows to ca. 4–5 µm after 5000 h (Figure 3b). It exhibits a multilayered structure, consisting of both an outward- and an inward-growing scale. The EDS elemental mapping (Figure 3c) and the line scan (Figure 3d,e) reveal that the outward-growing oxide is rich in Ti at the interface to the molten Pb. XRD analysis confirms the presence of TiO_2 in both rutile (α-TiO_2, hcp) and anatase (β-TiO_2, bcc) phases. Beneath this, a very thin Al-rich oxide layer is observed, identified as alumina Al_2O_3 by XRD. The inward-growing part of the oxide scale is rich in Ti next to the original surface, followed by a region with interspersed TiO_2/Al_2O_3. The presence of Ti- and Al-oxides in this zone indicates oxygen inward diffusion and oxidation of both Ti and Al. Note that Nb is also present in the inward-growing oxide region, see line scan and mapping. Below the multilayer oxide scale, oxygen diffusion into the bulk material (oxygen diffusion zone—ODZ) is observed in the line scan (Figure 3e) and Pb penetration is evident from both the mapping (Figure 3c) and the BSE image taken at higher magnification (Figure 3d). This demonstrates that the oxide scale, though being an efficient diffusion barrier, is not completely protective after 5000 h. Finally, voids are detected beneath the oxide scale, which most likely result from an imbalance between the inward diffusion fluxes of O and Pb on the one hand and the outward diffusion fluxes of Ti and Al on the other hand.

Figure 4 presents the corrosion behavior of the γ-TiAl alloy TNM-B1 in liquid Pb at 700°C. Although an oxide scale has grown on the sample surface, the scale is not entirely stable, Pb penetrates locally into the material, and a corrosion attack with a depth of up to 160 µm is observed after 5000 h. Dissolution and Pb penetration proceed first along the β_0 and α_2 phases, while the entire TiAl alloy is affected for prolonged corrosion attack (Figure 4b). As shown in Figure 4a, the non-protective

oxide scale deteriorates in locations with corrosion attack. The elemental mapping in Figure 4b shows a region where the oxide scale is still present. Similar to the scale at 600°C, the multilayer oxide scale formed at 700°C consists of outward-growing Ti-oxide, a very thin Al-oxide layer at the location of the original sample surface, and an inward-growing mixture of Ti-oxide and Al-oxide. In contrast to 600°C, a thin Al-oxide layer covers the outward-growing Ti-oxide after exposure at 700°C and also the inward-growing oxide is enriched in Al at the interface to the bulk material.

3.3.2 | *GE 48-2-2*

Figure 5 provides representative images of the corrosion behavior exhibited by GE 48-2-2 at 600°C. After 1000 h, the TiAl alloy is covered and protected by a very thin oxide scale with some slightly thicker oxide nodules dispersed on the surface, see Figure 5a. After 2000 h of exposure to liquid lead at 600°C, the majority of the sample is covered by a thin Al-rich oxide layer, while localized areas exhibit significantly thicker oxidation zones with thicknesses reaching up to ~8 μm (Figure 5b). Small voids are found below the thin oxide scale, which most likely result from Al outward diffusion due to oxide scale formation. Figure 5c,d present more details on the thick oxide zones after 2000 h exposure. These regions consist of outward-growing Ti-oxide (TiO_2), an inward-growing oxide with interspersed TiO_2/Al_2O_3 and a slight Cr enrichment in the upper part, and an inner oxygen diffusion zone (ODZ). The sample exhibits no detectable penetration of Pb after 2000 h.

More severe corrosion is observed for the same material exposed to liquid Pb at 700°C. After 1000 h (Figure 6a), a rather thick oxide scale (up to 24 μm thick) covers the entire surface of GE 48-2-2. As demonstrated by the EDS elemental mapping in Figure 6b, the oxide scale exhibits outward-growing Ti-oxide and an inward-growing mixture of Al-oxide and Ti-oxide. In contrast to the exposure at 600°C, the oxidation front is not diffuse but clearly pronounced and shows an enrichment in Al. Below the oxide scale, the TiAl alloy is depleted in Al and small voids are formed. Pb penetration is not observed after 1000 h, indicating that the oxide scale is still protective.

As shown in Figure 6c,d, exposure of GE 48-2-2 at 700°C leads to severe corrosion after 2000 h. The formerly formed oxide scale is deteriorated (remnants can be found in some places) and Pb penetrates the TiAl alloy up to a depth of 230 μm, see Figure 6c. At the corrosion front, Pb attacks the Cr-rich β_0 phase first and then the corrosion attack proceeds via the

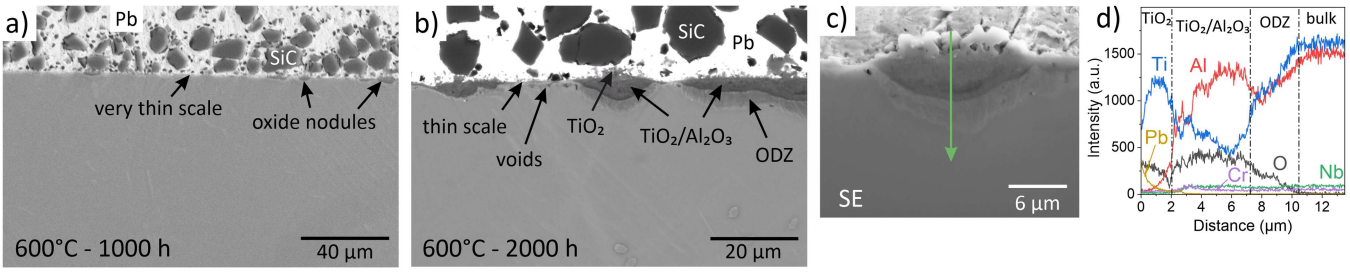

FIGURE 5 | GE 48-2-2 after exposure to Pb at 600°C (a) for 1000 h, (b, c) for 2000 h. (a) SE image, (b) BSE image, (c) SE image at higher magnification, (d) result of EDS elemental line scan along arrow in (c). [Color figure can be viewed at wileyonlinelibrary.com]

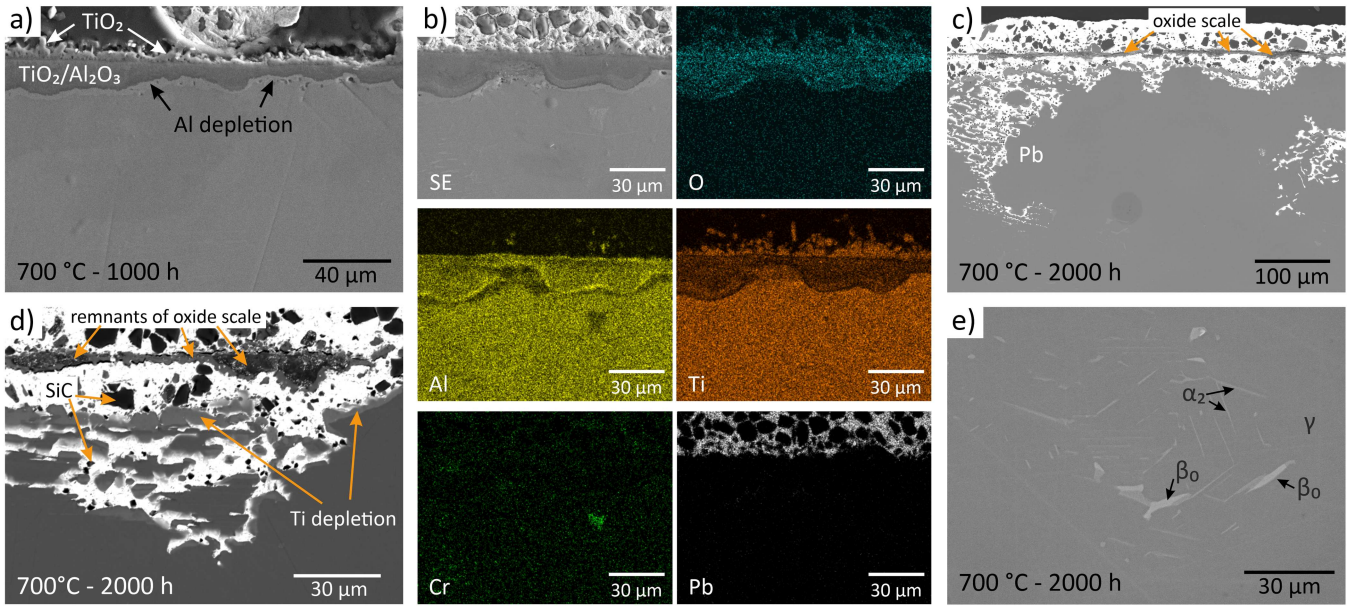

FIGURE 6 | GE 48-2-2 after exposure to Pb at 700°C (a, b) for 1000 h, (c–e) for 2000 h. (a) SE image, (b) EDS elemental mapping, (c–d) BSE images, (e) bulk microstructure. [Color figure can be viewed at wileyonlinelibrary.com]

Ti-rich α_2 lamellae. An image of the bulk microstructure is depicted in Figure 6e. In the regions closer to the sample surface that have experienced direct contact with Pb for a longer time, the remains of the TiAl alloy are depleted in Ti and enriched in Nb (Figure 6d), indicating selective dissolution of Ti.

3.4 | Discussion of TiAl Alloys

The multilayer oxide scale structure of GE 48-2-2 shares notable similarities with that observed on TNM-B1, consisting of an outward-growing Ti-rich oxide layer and an underlying mixed TiO_2/Al_2O_3 zone. For both alloys, an ODZ is observed below the inward-growing oxide zone at 600°C, while at 700°C the oxygen concentration shows a rather sharp drop at the interface between oxide and bulk and the oxide zone is enriched in Al at the oxidation front.

Despite the similarities between the γ-TiAl alloys regarding the oxide scale structure, there are also crucial differences. On TNM-B1, a continuous scale with rather homogeneous thickness grows at both temperatures. However, the scale is penetrable for Pb. At 600°C, small amounts of Pb are found directly below the scale, which still appears otherwise intact even after 5000 h. At 700°C, Pb penetration is much more severe. Pb corrosion and dissolution start along the β_0 and α_2 phase and extend to a depth of 160 μm after 5000 h. The formerly formed scale is destroyed. The more severe corrosion attack at 700°C compared with 600°C is caused by the higher solubility and faster diffusion at elevated temperature.

In contrast to the rather homogeneous oxide scale thickness on TNM-B1, an oxide scale with heterogeneous thickness develops on the alloy GE 48-2-2. At 600°C, extended regions with a very thin scale alternate with local thick oxide nodules. The presence of Cr in GE 48-2-2 might be responsible for the formation of the very thin scale, as Cr is known to promote the formation of Al_2O_3. In contrast to the Pb-penetrable scale on TNM-B1, both the thin scale and the oxide nodules formed on GE 48-2-2 at 600°C seem protective; Pb does not penetrate within 2000 h of exposure.

At 700°C, the oxide scale grown on GE 48-2-2 also varies strongly in thickness (though a very thin scale does not form) and becomes up to 24 μm thick already after 1000 h. After 2000 h, strong corrosion with an up to 230 μm deep penetration of Pb is found. Similar to TNM-B1, Pb attacks the β_0 phase first, then proceeds via the α_2 phase and finally corrodes the entire material. The obviously faster growth of the oxide scale on GE 48-2-2 at 700°C compared with TNM-B1 leads to its earlier failure. An oxidation study in air also reports a faster oxidation rate of GE 48-2-2 compared with TNM-B1 when exposed at 700°C [29]. In this publication, it is argued that Cr (present in GE 48-2-2 only) has a detrimental effect on the oxidation rate, while Nb (present in higher amounts in TNM-B1) is advantageous. According to the authors, Cr causes a higher number of defects in TiO_2 and thus a higher oxidation rate, while Nb reduces the number of defects in TiO_2 and leads to a lower oxidation rate. Although direct comparison of oxidation in air with corrosion in liquid Pb is not possible due to the different oxygen activities and corrosion mechanisms (interaction with Pb), the effect of Cr and Nb on the quality of TiO_2 formed at 700°C in the present study might be similar.

4 | Conclusion

In order to assess the material compatibility under conditions relevant for TES applications with liquid Pb as heat transfer fluid, the corrosion behavior of commercial Al-containing alloys in liquid Pb with 2E-7 wt.% dissolved oxygen was investigated for up to 5000 h at 600°C and 700°C. From two alloy families, two representatives were selected each, namely the ferritic FeCrAl alloys Kanthal APM and Kanthal APMT and the titanium aluminides TNM-B1 and GE 48-2-2. The following conclusions can be drawn from the results of the exposure tests:

- APM and APMT form a thin and protective Al-rich oxide scale at both temperatures, 600°C and 700°C. After 2000 h, the oxide scale on APMT is slightly thicker than the scale on APM.
- The oxide scale on APM remains intact and protective after 5000 h of exposure at 600°C. However, it becomes unstable at 700°C and internal oxidation is observed after 5000 h.
- A multilayer oxide scale composed of TiO_2 and Al_2O_3 forms on TNM-B1 at both 600°C and 700°C. At 600°C, the scale remains intact for at least 5000 h despite some Pb penetrating to the interface between scale and bulk material. At 700°C, oxide scale failure and severe Pb corrosion occur (160 μm deep after 5000 h).
- GE 48-2-2 shows a very thin oxide scale alternating with much thicker oxide nodules after exposure at 600°C. The scale is protective for at least 2000 h. At 700°C, a much thicker scale develops. For exposures exceeding 1000 h, the scale loses its protective properties and Pb penetration reaches a depth of 230 μm after 2000 h.
- For both titanium aluminides, the γ phase is the most corrosion-resistant phase, while β_0 and α_2 phases are attacked first.

Although excellent corrosion resistance is obtained for all materials at 600°C under the given conditions (2E-7 wt.% dissolved oxygen, stagnant Pb), longer exposure tests and tests under further conditions are recommended to confirm the applicability of the tested materials in liquid Pb at 600°C. The use of the γ-TiAl alloys in liquid Pb at 700°C is not recommended.

Acknowledgments

This research was funded by the German Federal Ministry for Economic Affairs and Climate Action (BMWK) under the grant number 03EE5050C. Open Access funding enabled and organized by Projekt DEAL.

Conflicts of Interest

The authors declare no conflicts of interest.

Data Availability Statement

Energy Storage (EST2). The data that support the findings of this study are available from the corresponding author upon reasonable request.

References

1. K. Vignarooban, X. Xu, A. Arvay, K. Hsu, and A. M. Kannan, "Heat Transfer Fluids for Concentrating Solar Power Systems—A Review," *Applied Energy* 146 (2015): 383–396, https://doi.org/10.1016/j.apenergy.2015.01.125.

2. A. Heinzel, W. Hering, J. Konys, et al., "Liquid Metals as Efficient High-Temperature Heat-Transport Fluids," *Energy Technology* 5 (2017): 1026–1036, https://doi.org/10.1002/ente.201600721.

3. K. Niedermeier, "A Perspective on High-Temperature Heat Storage Using Liquid Metal as Heat Transfer Fluid," *Energy Storage* 5 (2023): e530, https://doi.org/10.1002/est2.530.

4. J. Zhang, "A Review of Steel Corrosion by Liquid Lead and Lead–Bismuth," *Corrosion Science* 51 (2009): 1207–1227, https://doi.org/10.1016/j.corsci.2009.03.013.

5. *Handbook on Lead-bismuth Eutectic Alloy and Lead Properties, Materials Compatibility, Thermal-hydraulics and Technologies* (OECD Publishing, 2015).

6. A. Heinzel, G. Müller, and A. Weisenburger, "Behavior of Welds in Liquid Lead Containing 10 wt%–6 wt% and 10 wt%–8 wt% Oxygen," *Journal of Nuclear Materials* 437 (2013): 116–121, https://doi.org/10.1016/j.jnucmat.2013.01.298.

7. G. Müller, G. Schumacher, and F. Zimmermann, "Investigation on Oxygen Controlled Liquid Lead Corrosion of Surface Treated Steels," *Journal of Nuclear Materials* 278 (2000): 85–95, https://doi.org/10.1016/S0022-3115(99)00211-1.

8. A. Weisenburger, C. Schroer, A. Jianu, et al., "Long Term Corrosion on T91 and AISI1 316L Steel in Flowing Lead Alloy and Corrosion Protection Barrier Development: Experiments and Models," *Journal of Nuclear Materials* 415 (2011): 260–269, https://doi.org/10.1016/j.jnucmat.2011.04.028.

9. H. Wang, X. Qiu, Y. Li, et al., "Short-Term Corrosion Behavior and Mechanism of 316 Stainless Steel in Liquid Pb at 650 and 750°C," *Journal of Materials Engineering and Performance* 33 (2024): 7210–7221, https://doi.org/10.1007/s11665-023-08479-z.

10. A. Purwitasari, C. Oskay, A. Heinzel, R. Fetzer, A. Weisenburger, and G. Müller, "Corrosion of Austenitic Stainless Steels in Liquid Pb With 2E-7 Wt% Oxygen at 600 and 700°C," *Corrosion Science* 244 (2025): 112651, https://doi.org/10.1016/j.corsci.2024.112651.

11. A. Purwitasari, R. Fetzer, A. Heinzel, C. Oskay, A. Weisenburger, and G. Müller, "Pb Corrosion of Ferritic/Martensitic Steels at 600–700°C," *Corrosion Science* 255 (2025): 113142, https://doi.org/10.1016/j.corsci.2025.113142.

12. R. Wang, X. Qiu, S. Gao, et al., "Corrosion Behavior of 316 Stainless Steel Arc Parts in Liquid Lead at 650°C Under High Oxygen Concentrations," *RSC Advances* 12 (2022): 32700–32707, https://doi.org/10.1039/D2RA05165F.

13. H. Shi, A. Jianu, A. Weisenburger, et al., "Corrosion Resistance and Microstructural Stability of Austenitic Fe–Cr–Al–Ni Model Alloys Exposed to Oxygen-Containing Molten Lead," *Journal of Nuclear Materials* 524 (2019): 177–190, https://doi.org/10.1016/j.jnucmat.2019.06.043.

14. P. Dömstedt, M. Lundberg, and P. Szakálos, "Corrosion Studies of a Low Alloyed Fe–10Cr–4Al Steel Exposed in Liquid Pb at Very High Temperatures," *Journal of Nuclear Materials* 531 (2020): 152022, https://doi.org/10.1016/j.jnucmat.2020.152022.

15. H. Shi, R. Fetzer, C. Tang, et al., "The Influence of Y and Nb Addition on the Corrosion Resistance of Fe-Cr-Al-Ni Model Alloys Exposed to Oxygen-Containing Molten Pb," *Corrosion Science* 179 (2021): 109152, https://doi.org/10.1016/j.corsci.2020.109152.

16. H. Shi, R. Fetzer, A. Jianu, et al., "Influence of Alloying Elements (Cu, Ti, Nb) on the Microstructure and Corrosion Behaviour of AlCrFeNi-Based High Entropy Alloys Exposed to Oxygen-Containing Molten Pb," *Corrosion Science* 190 (2021): 109659, https://doi.org/10.1016/j.corsci.2021.109659.

17. E. Miorin, F. Montagner, V. Zin, et al., "Al Rich PVD Protective Coatings: A Promising Approach to Prevent T91 Steel Corrosion in Stagnant Liquid Lead," *Surface and Coatings Technology* 377 (2019): 124890, https://doi.org/10.1016/j.surfcoat.2019.124890.

18. A. Heinzel, R. Fetzer, F. Lang, et al., "Corrosion Tests on Austenitic Samples With Alumina and Alumina-Forming Coatings in Oxygen-Containing Stagnant Pb and Turbulently Flowing Pbbi," *Journal of Nuclear Materials* 596 (2024): 155121, https://doi.org/10.1016/j.jnucmat.2024.155121.

19. P. Dömstedt, M. Lundberg, and P. Szakalos, "Corrosion Studies of Low-Alloyed FeCrAl Steels in Liquid Lead at 750°C," *Oxidation of Metals* 91 (2019): 511–524, https://doi.org/10.1007/s11085-019-09896-z.

20. A. Purwitasari, R. Fetzer, A. Heinzel, C. Oskay, A. Weisenburger, and G. Müller, "Influence of Aluminizing and Pre-Oxidation on Corrosion Behavior of 316Ti in Liquid Pb at 600–700°C," *Corrosion Science* 251 (2025): 112896, https://doi.org/10.1016/j.corsci.2025.112896.

21. J. Lim, H. O. Nam, I. S. Hwang, and J. H. Kim, "A Study of Early Corrosion Behaviors of FeCrAl Alloys in Liquid Lead–Bismuth Eutectic Environments," *Journal of Nuclear Materials* 407 (2010): 205–210, https://doi.org/10.1016/j.jnucmat.2010.10.018.

22. M. Del Giacco, A. Weisenburger, A. Jianu, F. Lang, and G. Mueller, "Influence of Composition and Microstructure on the Corrosion Behavior of Different Fe–Cr–Al Alloys in Molten LBE," *Journal of Nuclear Materials* 421 (2012): 39–46, https://doi.org/10.1016/j.jnucmat.2011.11.049.

23. C. Cionea, M. D. Abad, Y. Aussat, D. Frazer, A. J. Gubser, and P. Hosemann, "Oxide Scale Formation on 316L and FeCrAl Steels Exposed to Oxygen Controlled Static LBE at Temperatures Up to 800°C," *Solar Energy Materials and Solar Cells* 144 (2016): 235–246, https://doi.org/10.1016/j.solmat.2015.09.007.

24. M. P. Popovic, A. M. Bolind, Y. Aussat, A. J. Gubser, and P. Hosemann, "Oxidative Passivation of Fe–Cr–Al Steels in Lead-Bismuth Eutectic under Oxygen-Controlled Static Conditions at 700° and 800°C," *Journal of Nuclear Materials* 523 (2019): 172–181, https://doi.org/10.1016/j.jnucmat.2019.06.004.

25. R. Xu, M. Li, and Y. Zhao, "A Review of Microstructure Control and Mechanical Performance Optimization of γ-TiAl Alloys," *Journal of Alloys and Compounds* 932 (2023): 167611, https://doi.org/10.1016/j.jallcom.2022.167611.

26. N. Mogale, W. Matizamhuka, and P. Cobbinah, "Hot Corrosion and Oxidation Behaviour of TiAl Alloys During Fabrication by Laser Powder Bed Additive Manufacturing Process." in *Corrosion - Fundamentals and Protection Mechanisms*, eds. A. F. Zafar, Dr., E. Ghosal, and Sharmin (IntechOpen, 2021). https://doi.org/10.5772/intechopen.100345.

27. Y. Liu, H. E. Ge, Q. S. Ren, et al., "Improved Corrosion Resistance of TiAlCrNbMo Alloy to Lead-Bismuth Eutectic by Pre-Oxidation," *Journal of Materials Research and Technology* 28 (2024): 707–718, https://doi.org/10.1016/j.jmrt.2023.12.044.

28. B. Jönsson, R. Berglund, J. Magnusson, P. Henning, and M. Hättestrand, "High Temperature Properties of a New Powder Metallurgical FeCrAl Alloy," *Materials Science Forum* 461–464 (2004): 455–462, https://doi.org/10.4028/www.scientific.net/MSF.461-464.455.

29. L. Mengis, A. S. Ulrich, P. Watermeyer, C. H. Liebscher, and M. C. Galetz, "Oxidation Behaviour and Related Microstructural Changes of Two β0–phase Containing TiAl Alloys Between 600°C and 900°C," *Corrosion Science* 178 (2021): 109085, https://doi.org/10.1016/j.corsci.2020.109085.